DOE/SF/20144—T3

FINAL REPORT

NATIONAL LASER USER'S FACILITY
UNIVERSITY OF ROCHESTER
LABORATORY FOR LASER ENERGETICS
U.S. Department of Energy Grant # DE-FG03-93SF20144

TITLE: Temperature-Dependent Tensile Strength, Surface Roughness Diagnostics, and Magnetic Support and Positioning of Polymer ICF Shells

Principal Investigator: Arnold Honig, Physics Dept, Syracuse University
Co-Investigator at L.L.E: Roger Q. Gram
Contributors to the work at Syracuse: M. Dong, Q. Fan, C.-K. Hsu and X. Wei

Period: October 1, 1993 - April 30, 1995.

December 15, 1995

DLC

FINAL REPORT

U.S. Department of Energy NLUF Grant # DE-FG03-93SF20144

TITLE: Temperature-Dependent Tensile Strength, Surface Roughness Diagnostics, and Magnetic Support and Positioning of Polymer ICF Shells

Principal Investigator: Arnold Honig, Phys. Dept, Syracuse University, Syr., NY 13244
Co-Investigator at L.L.E: Roger Q. Gram
Contributors to the work at Syracuse: M. Dong, Q. Fan, C.-K. Hsu and X. Wei

Period: October 1, 1993 - April 30, 1995.
Report preparation date: December 15, 1995

ABSTRACT

During the course of this grant, we perfected emissivity and accommodation coefficient measurements on polymer ICF shells in the temperature range 250 to 350 K. Values for polystyrene shells are generally between 10^{-2} and 10^{-3}, which are very advantageous for ICF at cryogenic temperatures. Preliminary results on Br doped target shells indicate an accommodation coefficient, presumably associated with surface roughness on an atomic scale, about an order of magnitude larger than for ordinary polystyrene target shells. We also constructed apparatus with optical access for low temperature tensile strength and emissivity measurements, and made preliminary tests on this system. Magnetic shells were obtained both from GDP coating and from doping styrene with 10 nanometer size ferromagnetic particles. The magnetic properties were measured through electron spin resonance (ESR). These experiments confirm the applicability of the Curie law, and establish the validity of using ESR measurements to determine shell temperature in the low temperature regime from 4K to 250K, thus complementing our presently accessible range. The high electron spin densities ($>10^{20}/cm^3$) suggest magnetic levitation should be feasible at cryogenic temperatures. This work has resulted in two conference presentations, a Technical Report, a paper to be published in Fusion Technology, and a Master's Thesis.

I. INTRODUCTION

In this report, we describe the work in our laboratory at Syracuse supported by NLUF during the grant period. Our activities represent a continuing effort on our part on problems related to the inertial confinement fusion (ICF) program. Our investigations began with a multifaceted program aimed at preparing and imploding polystyrene targets containing solid spin-polarized D_2 fuel. This program was brought to an advanced stage, including cold (4K) transfer of solid deuterium-filled target shells prepared at Syracuse and transported, positioned and shot at the OMEGA facility at the University of Rochester's Laboratory for Laser Energetics (LLE). Due to the shutdown of OMEGA for its upgrade, the final experiments using spin-polarized solid D_2 targets were not completed[1]. Nevertheless, the entire deuterium polarization technology has now been fully developed and demonstrated[2] and the impetus for spin-polarized fusion has not diminished. It is most probable that the polarized fuel technology we developed will be utilized again within the next few years. In addition, the 4K cold-transfer[3] technology we introduced formed the basis of the current cryotarget development for OMEGA upgrade. In the course of this earlier work, we developed a strong capability for characterizing polymer target shells by techniques not readily accessible at other centers, and since the closing of (old) OMEGA, we have focused our attention on target shell properties such as emissivity and accommodation coefficient, which are of high concern to the cryogenic ICF program, both for polarized and unpolarized fuels. In direct drive ICF experiments, the emissivity determines the warm-up rate under room temperature black-body irradiation during the short interval between retracting the shroud, in order to make the target accessible to the laser beams, and the firing of the lasers. Since there are mechanical constraints which limit the speed with which the shroud can be retracted and since the black body radiation environment is difficult to alter, emissivity controls the target shell temperature rise. For polarized targets, an appreciable temperature rise leads to relaxation-induced depolarization, and must be avoided. For an unpolarized target, the temperature rise must also be held to a very low value to avoid distortion of the required

highly-symmetrized condensed fuel layer. For a given residual gas pressure in the fusion chamber, a low accommodation coefficient[4] reduces the temperature rise rate due to free molecular conduction. Even with indirect drive, shell warming from black-body radiation cans be a significant detrimental factor. Both emissivity and accommodation coefficient are less than or equal to 1, and lower values of these, which result in slower warming of the target, are always advantageous to ICF for the reasons presented above. In this past year, we improved upon the techniques we first introduced at the Monterey Ninth Target Specialists' meeting[5] in 1993, and more recently at the Albuquerque Tenth Target Specialists' meeting[6], for investigation of emissivity and accommodation coefficients of target shells. The improvements are principally with respect to target conductive thermal isolation and optical access. Our measurements of both emissivity and accommodation coefficient are reliable and in the vicinity of 10^{-2}, a very satisfactory range for temperature stability of polystyrene-based cryogenic ICF targets.

Also included in this report are initial experiments on magnetic properties of shells, obtained by doping styrene with magnetic particles of a few nm diameter prior to forming the shells by a microencapsulation or drop tower method. Experiments on paramagnetic shells obtained by stabilization at low temperatures of paramagnetic defects produced by gas discharge plasma (GDP) coatings were initiated, as was consideration of using room temperature stable organic radical dopants[7] in styrene to make paramagnetic polystyrene shells. The paramagnetism with which the shells become endowed permits contactless temperature sensing via electron spin resonance (ESR) measurements, owing to the Curie law. These measurements are applicable all the way down to the liquid helium temperature region, enabling extension of our target shell emissivity and accommodation coefficient measurements to the temperature region where they will be actually employed. Other applications interesting to ICF are levitation of target shells at low temperatures for non-perturbative shell positioning and possibly shell transport, and uniform or possibly even profiled shell heating in the liquid hydrogen temperature range through electron spin resonance and relaxation.

II. EMISSIVITY AND ACCOMMODATION COEFFICIENT MEASUREMENTS ON POLYSTYRENE ICF TARGET SHELLS

Despite the importance of emissivity measurements both for direct and indirect drive inertial confinement fusion, as mentioned in the preceding section, our measurements are to our knowledge the first for polystyrene polymer shells, which at present are considered an essential component of the ICF target shell program. In this section, we review the theory and experiments we have carried out on emissivity and accommodation coefficient of polystyrene target shells filled with both helium and deuterium gas. A substantial amount of the material presented here has been previously described at conferences[5,6], in a Technical Report[8], and in a publication submission[9], but new material is also contained in this report.

In this section, we first describe the method and apparatus, then the theoretical basis of the measurements, next the experimental results for a variety of shells, and finally we present a discussion of the techniques and the results.

A. Description of the Method and Apparatus

The experiments are thermal transfer ones in which a shell of known heat capacity is subject to warming from a known isothermal environment, in our case the wall of the cell containing the target shell. This wall, at temperature T_W, is maintained warmer than the shell temperature, T_S. The shell is mounted on very thin spider silks, and hence is thermally isolated with respect to heat conduction from its support structure. Thus, heat transfer to the shell is via net radiation absorption and via gas conduction. The radiative heat transfer rate is proportional to $e_S(T_W^4 - T_S^4)$, where e_S is the shell emisivity. The gas pressure is arranged to be always low, so that the heat transfer rate via gas conduction is characteristic of the molecular free conduction (as opposed to diffusion) regime. Its contribution to the heat transfer rate is proportional to $a_S P_C (T_W - T_S)$, where a_S is the accommodation coefficient[4] of the shell and P_C is the gas pressure in the cell. Because of the different heat-transfer-rate temperature dependencies, and the ability to control the pressure range, separation of the contribution of each of these thermal transport mechanisms to the temperature rise of the shell can be effected by monitoring the target

shell temperature during warm-up. The innovative element of these experiments is in the means of monitoring the shell temperature, T_S. The shells are very small and any external thermometer placed in contact with them would compromise the conductive isolation and make the interpretation of the measurements difficult, or indeed even impossible. We introduced a method whereby the property of a shell called its permeability coefficient, which is proportional to the rate at which gas leaks out of the shell into a vacuum, serves as the thermometric indicator. This quantity, denoted by K_P, depends exponentially on the temperature of the shell. One simply measures the gas leakage *rate* out of the shell by continuously monitoring the pressure in its containment cell. This method works very well in the temperature region of 250 - 350K. Below 250K, the permeation rate is too slow. Nevertheless, these 'high' temperature values are helpful for approximating the low temperature values, and we have proposed other contactless temperature determination methods for shells which can be utilized for very low temperature versions of these experiments. Among these are the magnetic susceptibility one, which has been mentioned above, and visual observation of phase transitions at boiling and melting points of various materials, which is described later in this report.

A polystyrene target shell is mounted on very low thermal conductance spider silks and placed in a small sample cell whose walls are maintained at any desired temperature, T_W, between 77K and 350K. The shell temperature, T_S, can be cooled to a low value, for example 77K, at which any gas inside it cannot leak out since the shell is very impermeable at low temperature. The sample chamber is connected via a thin tube to a larger volume which includes an accurate pressure sensor in the low pressure regime, in our case a Baratron operable over the pressure range 0 to 2000 Pa. The experimental arrangement, including provision for permeating gas into the shell, is shown in Fig. 1. In Fig. 2, one form of sample mounting, in which the shell is glued to 2 spider silks, is shown. This is the principal mounting method used in the experiments reported here. We have also successfully positioned shells freely on a net of spider silks, such as is shown in Fig. 3. In this way, the shells are usable after being characterized, and also accessible for visual viewing through an Indium o-ring sealed window at the bottom of the cell, in a manner depicted in Fig. 4. The aim is to cool the gas-filled target shell, quickly raise the

temperature, T_W, of the sample cell walls, and observe the rise in T_S due to heat transport from the cell walls to the shell. Using the known values of polystyrene heat capacity[10], $C_V(T)$, and measurement of shell temperature as a function of time during the warm-up, the total rate of heat absorption of the shell, dQ_S/dt, is obtained from the product $C_V(T)(dT_S/dt)$.

The procedure consists of permeating either helium or deuterium gas at room temperature (293K) into the target shell to about 12 atmospheres pressure. The liquid -N_2 filled bath is then raised so as to surround the sample cell, as shown in Fig. 1. The sample cell is next evacuated, but gas remains inside the target shells since the permeation coefficient is a very strong function of T, and at 77K, the polystyrene permeation time constant (inverse of the permeation rate) is essentially infinite with respect to the time scale of these experiments. The liquid-N_2 bath is then removed, and 1 minute later, the sample cell is immersed in the large bath filled with methanol at a selected temperature, which quickly brings the sample cell wall temperature, T_W, to that of the bath. During the 1 minute time interval between removal of the liquid-N_2 bath and immersion in the higher temperature methanol bath, the shell temperature, T_S, typically warms to a temperature which is below 150K, involving almost negligible gas leakage from the shell. However, a small amount of outgassing from the sample cell walls takes place, constituting a background leakage rate.

As the shell warms towards T_W by radiation and gas conduction from the sample cell walls, the gas in the shell starts to leak out. The resulting pressure, P, indicated by the Baratron, is monitored in time, and its rate of change provides a means of determining T_S. When T_W is equal to room temperature (the temperature of the Baratron space), the pressure in the sample cell, P_C, is equal to P. When the temperatures are different, P_C must be corrected for the transpiration effect[11]. We note that the volume of the Baratron plus sample cell is much larger than that of the shell. In this way, as the shell empties, the measured pressure remains sufficiently low for the condition of free molecular conduction to hold through most of the process.

B. Heat Transfer to Shell

We have already noted that the two principal thermal transport mechanisms which warm the cold shell when the sample cell wall is at temperature T_W are radiation and gas conduction in the molecular free conduction regime. For the radiative contribution, we have

$$\dot{Q}_S(RAD) = e_S\sigma A_S(T_W^4 - T_S^4), \quad (1)$$

where e_S is the emissivity of the target shell, σ is the Stefan-Boltzmann constant, equal to 5.67×10^{-12} W/cm^{2}K^4, and A_S is the area of the target shell. For gas conduction in the free molecular conduction regime, which for our geometry corresponds approximately to P<30Pa, we have

$$\dot{Q}_S(MOL\ \ FREE\ COND) = a_S\Lambda A_S P_C(T_W - T_S), \quad (2)$$

where $\Lambda=\Lambda_0(273/T_S)^{1/2}$, and the other quantities have already been defined. For reference, the free molecular conduction regime applies roughly when the mean free path, λ, exceeds about 0.1D, where D is the approximate distance between the cold (T_S) and warm (T_W) surfaces, and equals about 0.3 cm in our apparatus. At P = 1 Pa, $\lambda_{He}(273K)$ = 1.6 cm and $\lambda_{D2}(273)$ = 1.1 cm. The values of Λ_0 for He and D_2 gas, obtained from Ref. 4, are respectively 2.23 Wm^{-2}K^{-1}Pa^{-1} and 3.24 Wm^{-2}K^{-1}Pa^{-1}.

C. Shell Temperature Measurement

To analyze warm-up curves and obtain quantitative values of e_S and a_S, we must be able to determine the shell temperature, T_S, without a contact device. As remarked earlier, we do this through the temperature dependence of the instantaneous shell outgas rate, which is easily monitored with the Baratron.

The pressure p(t) inside a shell (at temperature T_S and initially filled to a pressure p_0) whose contained gas is permeating into a near vacuum falls off exponentially in time to nearly zero, provided that the volume of the shell is much less than the volume of the sample cell, as in our case. At equilibrium, the final shell pressure is equal to the Baratron

pressure, P_f, and is between 10 and 100 Pa, compared with ~12 atmospheres initial pressure of the shell. Since the measured Baratron pressure includes not only the gas permeated out of the shell but also a small component of background pressure resulting from outgassing of the call walls, which increases nearly linearly in time and thus is expressible as bt, the corrected pressure is P′ (= P - bt). Its expected time evolution is

$$P' = P_f'(1 - e^{-\frac{t}{\tau}}), \tag{3}$$

where τ, the time constant for permeation, is given[12] by

$$\tau = \frac{wr}{3K_P R T_S}. \tag{4}$$

w is the shell wall thickness, r the shell radius, K_p the permeation coefficient, and R the gas-constant. In Fig. 5, a series of experimental plots are shown from which values of τ are obtained using Eq. (3). Since K_p is an activated quantity with activation temperature α, we write the temperature dependent permeation coefficient

$$K_P(T_S) = K_P(293K)e^{-\alpha(\frac{1}{T_S} - \frac{1}{293})}, \tag{5}$$

and the temperature dependent τ as

$$\tau(T_S) = \tau(293K)\frac{293}{T_S}e^{+\alpha(\frac{1}{T_S} - \frac{1}{293})}. \tag{6}$$

With the calibration of the permeation time constant τ as a function of temperature, as in Fig. 5, it becomes a thermometric property for the shell. The assemblage of τ values is shown on a semi-log plot, in Fig. 6. The good fit to Eq. (6) provides confidence that it is a good thermometric property, even into the temperature extrapolation region where direct measurements of τ weren't made.

In the warm-up experiments, P′ and T_S both increase with time. The P′ vs t curve is generated directly from the Baratron pressure data, for several experimental runs at various sample cell wall temperatures, T_W, and is shown in Fig. 7. In order to obtain a T_S vs t derived curve, we calculate the instantaneous permeation time constant, τ, from the following simply derived equation:

$$\tau = \frac{P'_{final} - P'(t)}{\frac{dP'}{dt}}. \qquad (7)$$

dP′/dt is determined by fitting the P′ vs t curve in Fig. 7. to a 13 parameter function of exponentials. This fits the curves very well and permits easy calculation of derivatives. From the τ values, T is calculated from the data shown in Fig. 6. The results for the same series of sample cell wall temperatures, T_W, shown in Fig. 6, are illustrated in Fig. 8.

D. Results

We illustrate the graphical and analytical method used to determine the emissivity and accommodation coefficient for shell 1S, for which the relevant data have already been plotted in Figs. 7 and 8. Figs. 9A and 9B correspond respectively to the lowest and highest cell wall temperatures of the series. From the warm-up experimental curves, a data sheet is prepared. dQ_S/dt is calculated from the product of dT_S/dt and $C_V(T)$, with the latter evaluated from the known values of the specific heat of polystyrene[10] and the directly measured values of the shell mass. In this series of experiments, 3 μg were added to the shell mass for the (separately determined) mass of the glue, which is arbitrarily taken to have the same specific heat as polystyrene, with only a small error introduced from this simplification since the mass of the glue is only a small fraction of that of the shells used. Referring to Fig. 9, we see that all curves are plots of various quantities against (T_W^4 - T_S^4). Curve *a* is the experimental data plot with dQ_S/dt the ordinate. Curve *b* is the elapsed time plot, which one notes increases from right to left in this plot. Curve *c* is the plot of the pressure, P_C, which we emphasize is not corrected for background since gas conduction depends on total pressure regardless of its origin. P_C is equal to

$(T_W/293)^{1/2}$ P. The sample cell pressure is different from the measured Baratron pressure since the gas in the volume monitored by the Baratron is at room temperature whereas the gas in the sample cell is essentially at temperature T_W. The transpiration effect[11] gives the above relation between the actual pressures. Curve *d* represents the free molecular conduction, and is plotted from Eq. (2), using the value 1 for the accommodation coefficient. If radiation were the only heat transport mechanism, we would expect curve *a* to be a straight line passing through the origin. At the early times (right side of Fig. 8), this is nearly the case because P_C is small at early t when T_S is low. Curve *e* is generated by subtracting a suitable fraction of curve *d* from curve *a*, so that the resultant plot is linear and passes through the origin. That fraction is the accommodation coefficient. The accuracy obtained this way is about 10%, in the sense that without sophisticated data analysis, one can visually distinguish the departure from optimum linearity upon changing the accommodation coefficient by ±10%. After this fit is attained, emissivity is determined from the slope of curve *e*, in conjunction with Eq. (1).

The experiments have been carried out thus far with several wall temperatures for shell 1S (see Figs. 6 and 7), and with other polystyrene shells from different sources. Table I illustrates some of the results. For shell 1S, the emissivity and accommodation coefficient

TABLE I. EMISSIVITY AND ACCOMMODATION COEFFICIENT DETERMINATIONS

Shell	1S: He OD=945μm W=17μm MASS=50.1μg		1S: D_2		3S: D_2 OD=686μm W=6.5μm MASS=10.4μg	
Coeff. / T_W(K)	a_S	e_S	a_S	e_S	a_S	e_S
252	0.0037	0.016	0.0069	0.010		
273	0.0031	0.013	0.0025	0.019	0.0017	0.0060
283			0.0032	0.040		
287	0.0018	0.019				
290					0.0014	0.0061
313	0.0028	0.011	0.0030	0.014		
341	0.0027	0.012				

values are within the possible error margins, but a real temperature dependence for e_S and a_S cannot be excluded. The shell 3S, of smaller diameter and wall thickness than shell 1S, shows a significantly smaller e_S, which we believe results from lower absorption in its thinner walls.

E. Discussion

The emissivities and accommodation coefficients obtained have lower values than are usually encountered with other materials. However, recent calculations[13] of R. Stevens of General Atomics are apparently consistent with our emissivity values. Accommodation coefficients usually are larger for deuterium gas than for helium gas. This is not in evidence in our results. It is known that the accommodation coefficients become larger with increased surface roughness on an atomic scale, since an impinging molecule can then make many collisions on a single encounter with the surface. We tried to exploit this and measure possible surface roughness this way. Pairs of shells with similar dimensions were obtained, with one of the pair appearing 'rough' and the other 'smooth' under an optical microscope. We sought to test the possibility of a correlation of optically observed roughness with atomic scale roughness. No correlation has been observed, which is not too surprising since the optically evident imperfections were on a scale of microns. Two shells underwent an SEM scan after their emissivity measurements, but no conclusive correlations were found there either.

Brominated styrene shells, sometimes known as "hairy" brominated shells, are expected on an atomic scale to be considerably rougher than normal polystyrene, or parylene-coated polystyrene. Some of these were kindly sent to us by Bob Cook, of Lawrence Livermore National Laboratory (LLNL). Fig. 10 shows a comparison at comparable cell wall temperatures of the warm-ups of a brominated shell (Fig. 10A) with that of shell 1S (Fig. 10B), a pure polystyrene smooth shell of comparable diameter. Interestingly, the accommodation coefficients differ by an order of magnitude but the emissivities vary by less than a factor of 2. The surface roughness property is supposed to be reversible with suitable washing treatment. The one experiment in this regard that

we undertook failed to result in an appreciable change in the accommodation coefficient. More experimental work is planned on the brominated shells.

A few shell warm-up experiments yielded anomalous results. In these, the temperature rise curve, such as typified by Fig. 8, was distorted, and extrapolation to the final temperature did not correspond to the actual wall temperature. In these cases, the P vs t curves also displayed slight breaks and oscillations in slope. These are explained in terms of gas other than from the shell getting into the cell, either from a small leak or from outgassing as a consequence of contaminated gas (with air, for example) or contaminated lines (oil, for example), which could affect the desorption on thermal cycling. In one case, we identified a thermal desorption problem attributable to a particular hard solder, a silver/phosphorous/copper alloy, used at a joint to extend a pumping line. Another anomalous result concerned the value of the permeation coefficient, K_P, for a few of the many shells studied. The relation between the permeation coefficient of a thin-walled spherical shell of a given material and the observed permeation time constant, τ, is given by Eq.(4).. Using our experimental values of τ, and measured values of the shell parameters w and r, K_P can be determined. One way to display the constancy of K_P is shown in Fig. 11, where all measured polystyrene shell points would lie on the same straight lines of slope K_P. Departures for two of our shells, 1R (visually 'rough' under an optical microscope) and 2S (smooth), from the straight lines generated by the other points suggest deviant effective K_P values for those shells. Experiments with D_2 gas were not done with these shells since they broke prematurely, but there is little reason to believe the behavior would be different. We do not fully understand these results, but can speculate that a larger than expected effective K_P could result from microscopic imperfections in the shell wall, and that a smaller than expected effective K_P could be due a thin layer of PVA adhering to part of the shell surface.

Contactless thermometry measurements described in this work, which are based upon temperature-dependent permeation of gas out of a shell, have a limited working temperature range between about 250K and 350K for polystyrene, and an even higher temperature range for other less permeable polymers. The application of these results is principally intended for cryo-targets, and it would be useful to extend contactless

thermometry to lower temperatures. Several visual methods have been proposed involving optical access, such as visual observation of phase transitions for specific gases, visual observation of change in size of a shell as the pressure changes with temperature according to the gas law, and interference determinations of shell size. These all have special problems associated with them but are not entirely devoid of promise. For this reason, and for other experiments as well where optical access is advantageous, we constructed a sapphire-windowed cell inside of which was supported a spider silk net which holds a target shell. Schematic drawings were shown in Figs. 3 and 4. A long distance microscope[14] and CCD camera have been installed to operate with this system, as shown in Fig. 12. Later, the viewing system will be used in conjunction with a windowed variable-temperature cryostat for low temperature experiments Down to 4K. Shells which have been prepared to be paramagnetic also allow emissivity measurements down to the liquid helium temperature range. Our experiments with such paramagnetic shells are described in the next section.

III. MAGNETIC POLYSTYRENE SHELLS

It has long been known that GDP (gas discharge plasma) coated shells contain high densities of paramagnetic centers on the shell right after coating, which have very limited lifetimes (order of hours) at room temperature. With shells provided by Dr. Bob Cook of Lawrence Livermore National Laboratory (LLNL) shipped to Syracuse overnight in dry ice, we have investigated the ESR signals as a function of shell temperature, and as a function of shell storage time at different temperatures. Electron spin densities up to $10^{20}/cm^3$, line widths, and T_1 values (spin-lattice relaxation times), have been determined. These ESR features can impact the ICF program by providing contactless thermometric methodology based on the Curie law for shell temperature determination, by providing a means of magnetic shell levitation, and by making possible uniform or profiled shell heating through the electron spin relaxation coupling to the lattice..

In view of the time instability of the paramagnetism of the GDP coated shells and the need to operate at near liquid hydrogen or liquid helium temperature regions for sufficiently large paramagnetic susceptibility for some of the above-mentioned

applications, we pursued other courses as well. We undertook to dope styrene with 10 nm size magnetite (Fe_2O_3) particles and process the resultant material into shells. This was done successfully at LLNL by Bob Cook using the drop tower method, and was attempted unsuccessfully (only one attempt) at LLE, using the microencapsulation method. Both methods certainly can be improved by diluting the magnetic particles, since the styrene was doped to very near the concentration limit where precipitation out of the carrier fluid occurs. A third method we have been considering is to incorporate stable organic radicals in the styrene, such as is done to make dynamically spin-polarized nuclear targets[7] for nuclear and particle physics experiments. This method is not discussed in detail here since experimental work has not yet begun. One notes that this last method solves the time stability problem of the paramagnetism, but of course still requires cryogenic temperatures for the magnetization to be an appreciable fraction of the saturation magnetization in available magnetic fields. .

A. Paramagnetism of GDP Plasma Coated Shells

The GDP coated shells retain their paramagnetism almost indefinitely when kept at liquid N_2 temperatures, and thus are readily accessible for an experimental program. However, the paramagnetism lifetime is only about an hour at room temperature, and since experimental preparations generally require some residence time at room temperature, a shell's paramagnetism becomes degraded to some degree with each experiment. The instrument we used for most of the ESR measurements is a commercial Varian X-band ESR spectrometer, with a continuous flow liquid helium cooling system. A schematic drawing of its essentials is shown in Fig. 13. We also have assembled our own K-band ESR system in which a shell can be placed directly inside a liquid helium cryostat, allowing measurements to lower temperatures than possible in the continuous flow system. This has not as yet been used for shell experiments.

A typical ESR spectrum taken at a temperature of 15K of a single fresh shell is shown in Fig. 14A. The X-band microwave power used was 0.01 mW. The electron's g-factor is 1.999, and the line width is 24 G. By comparing the integrated signal intensity with that of a known sample of pitch, the spin density was determined to be about $5X10^{19}/cm^3$. The T_1

was determined from the saturation method, and found to be $3X10^{-4}$ s at the temperature 15K. The spin density decay time for this shell is about 80 minutes at room temperature, a few days at dry-ice temperature, and longer than a month at 77K. There are some variations in these parameters among different types of shells, but these have not yet been systematically studied. The thermometric property is clearly demonstrated from our experiments, with the observed equilibrium integrated ESR signal proportional to T^{-1}, as expected from the Curie law. Effective microwave shell heating prospects are also supported by the measured spin-lattice relaxation time (T_1) value. At 15K and in a 15T magnetic field, most of the electron spins would be highly polarized. Each spin transition absorbs hν energy from a microwave photon, amounting to about $6X10^{-17}$ ergs. With $5X10^{19}$ spins/cm^3, about $3X10^3$ ergs/cm^3 is absorbed for a single absorption transition allotted to each electron. For a T_1 of $3X10^{-4}$ s, one can have about $3X10^3$ transitions per second, delivering up to 1W of power per cm^3 of polymer shell. For a shell of 1 mm diameter and 30 μm wall thickness, this amounts to 10 mW, a fairly substantial power. In fact, T_1 for electronic spins frequently decreases quadratically or faster with increase of field, and the T_1 we used in the above calculation corresponds to the measured one at 3 kG. Thus, 10 mW may be a considerable underestimate of the deliverable power. This feature can of course be utilized in high B field environments separate from OMEGA, for example in preparation of smooth fuel surfaces in target shells. Finally, with regard to levitation, using the value 10^{-23}J/T for the Bohr magneton, the magnetic moment of 1 cm^3 of polymer with $5X10^{19}$ spins/cm^3 is $5x10^{-4}$ J/T. In a readily accessible magnetic field gradient of 100T/m, the force exerted on 1 cm^3 of polymer is $5X10^{-2}$ Newtons. This is 5 times the weight, 10^{-2} Newtons, of 1 cm^3 of polymer. Thus, with paramagnetic densities for shells which we have observed (and which are not the maximum attainable), levitation is a feasible prospect at 15K and high magnetic fields. Although difficult to attain, such field values may be possible in OMEGA, with an appropriate ported spherical insert of about 30 cm diameter, and computer-derived windings within a complex topography (to leave clear laser beam access). High T_C superconducting windings may find a use here when they attain the necessary current densities. In such an environment suitable for levitation, an alternative route to our previous efforts towards polarized nuclear fuel

fusion may also be possible through dynamic polarization employing combined NMR and ESR on deuterated (and tritiated) polymer shells or foams.

B.. Shells Made from Magnetite-Doped Polystyrene

Our efforts in this endeavor succeeded in making the proper doped styrenes, but there has been only limited success is fabricating shells. Only a few useful shells were obtained from the drop-tower production method, which were very fragile. The spin-resonance signal could be measured, but they were of very limited use in containing gas. They did show characteristic ferromagnetic resonance behavior, in particular very little temperature dependence of the integrated resonance signal. This is of course what we wanted, namely a high magnetization at room temperature. A typical resonance signal is shown in Fig. 14B. The microencapsulation attempt at LLE failed at the first (and only) try thus far, and has not yet been re-attempted due to a busy schedule of preparing targets for OMEGA upgrade. We expect a modest effort to be resumed. We believe that by diluting the magnetite a factor of between two and ten, both experiments will succeed and provide magnetic, gas-retaining shells.

We describe now the preparation of the styrene for each of the shell formation methods, since the mixtures of styrene and solvents used for each method differ. At the outset, we express appreciation for the extensive efforts, eventually successful, made by Dr. Raj and Dr. Aziz of the Ferrofluidics Corporation to find suitable surfactants for the magnetite in the chemical environments we required for the shell production. The styrenes were obtained from Pressure Chemical Corporation of Pittsburgh.

The drop-tower method required a low molecular weight styrene (90,000). The composition of the material used for the drop tower process was:

Magnetite:	8.3% by weight
Oil Soluble Dispersant:	1.5 to 4.5% by weight
Carrier Liquid (I-Propanol and Dichloromethane):	82.2 to 85.2% by weight
Low Molecular Weight Styrene Polymer"	5% by weight

The microencapsulation method required a high molecular weight styrene (207,000). The material used for the microencapsulation process was:

Magnetite:	8.0% by weight
Oil Soluble Dispersant:	1.5 to 4.5% by weight
Carrier Liquid (Benzene and 1,2 Dichlorethane)	80 to 83% by weight
High Molecular Weight Styrene Polymer	7.5% by weight

Handling and shipping of the drop-tower mixture was more difficult than for the microencapsulation mixture, since the former is very volatile and perfect seals in allowable shipment containers were hard to obtain. The initial shipment was successful, but storage over a considerable time period resulting in evaporation to the point where it was difficult to reconstitute the material. Extra material is still available at Syracuse, and further attempts will be made.

IV. Summary

A program on characterization of ICF target shells with respect to their emissivity and accommodation coefficients has been carried out for the first time. The results are favorable to maintaining temperature stability of the fusion fuel while the targets are subjected to room temperature radiative heating and possibly gas conductive heating just prior to the laser shot. A net-type shell support inside an optically accessible cell has been constructed which in conjunction with a long-distance microscope, allows new shell characterization experiments. We have also begun experimentation on ICF target shells made paramagnetic by GDP plasma coating, and by doping with paramagnetic or magnetic impurities styrene from which target shells are made. These offers promise for extending emissivity measurements to cryogenic temperatures, and possibilities for target shell levitation and other applications.

REFERENCES:

1. FINAL REPORT, U. S. Dept. of Energy NLUF GRANT DE-PS03-91SF18892, December 17, 1993.

2. A. Honig, Q. Fan, X. Wei, A. M. Sandorfi and C. S. Whisnant, Proceedings of the Seventh International Workshop on Polarized Target Materials and Techniques, Bad Honnef, Germany, June 20 - 22, 1994. Nuc. Instrum. and Meth. A356, 39 (1995).

3. N. Alexander, J. Barden, Q. Fan, and A. Honig, Rev. Sci. Instrum.62, 2729 (1991).

4. A. Roth, Vacuum Technology, 2nd Ed. North Holland Publishing Company, Amsterdam, 1982. The accommodation coefficient is the fraction of the maximum transferable "hot" molecules's energy imparted to the cold target shell upon collision..

5. A. Honig, NEW POLYMER TARGET-SHELL PROPERTIES AND CHARACTERIZATIONS, Ninth Target Fabrication Specialists' Meeting, Monterey, CA. July 6-8, 1993.). July 6-8, 1993. Monterey, CA. CONF-9307127 L-15854-2.4.

6. A. Honig, EMISSIVITY AND ACCOMMODATION COEFFICIENT OF POLYMER TARGET SHELLS, Tenth Target Fabrication Specialists' Meeting,, Albuquerque, NM. Feb 6-10, 1995. Compiled by Larry R. Foreman and Jean C. Stark, Los Alamos National Laboratory. Publication number LA-UR-95-29386.

7 . See, for example, article by Bunyatova, and two by van den Brandt et al., on p. 29, 34 and 36 of Proceedings of the Seventh International Workshop on Polarized Target Materials and Techniques, Bad Honnef, Germany, June 20 - 22, 1994. Nuc. Instrum. and Meth. A356, (1995).

8. A. Honig, Q. Fan, C.-K. Hsu and X. Wei, HEAT TRANSFER PROPERTIES OF POLYMER TARGET SHELLS AT TEMPERATURES BETWEEN 250K AND 350K, TECHNICAL REPORT #1, U. S. Department of Energy NLUF Grant # DE-FG03-03SF20144, March 1995.

9. A. Honig, Q. Fan, C.-K. Hsu and X. Wei, to be published in FUSION TECHNOLOGY, 1996.

10. J. Brandrup and E. H. Immergut, Eds., POLYMER HANDBOOK, 3rd Edition. John Wiley and Sons, New York.

11. See Ref. 4 above, p. 53.

12. L. A. Scott, R. G. Schneggenburger and P. R. Anderson, J. Vac. Sci. Technol. A4, 1155 (1986)..

13. Private communication from R. Fagaly and R. Stevens, of General Atomics Corp., Feb. 1995.

14. Infinity Model K-2 Long-Distance Microcsope, from Infinity Photo-Optical Company, Boulder, CO. Available from Edmund Scientific Company.

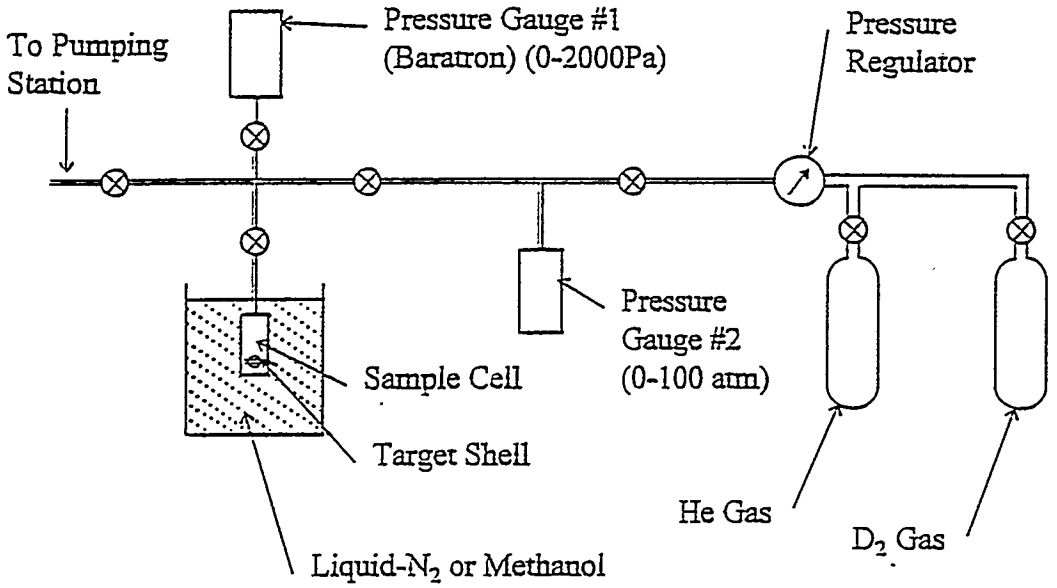

Fig. 1. ICF target shell permeation apparatus for measuring shell emissivity and accommodation coefficient in the temperature range 230 - 350 K.

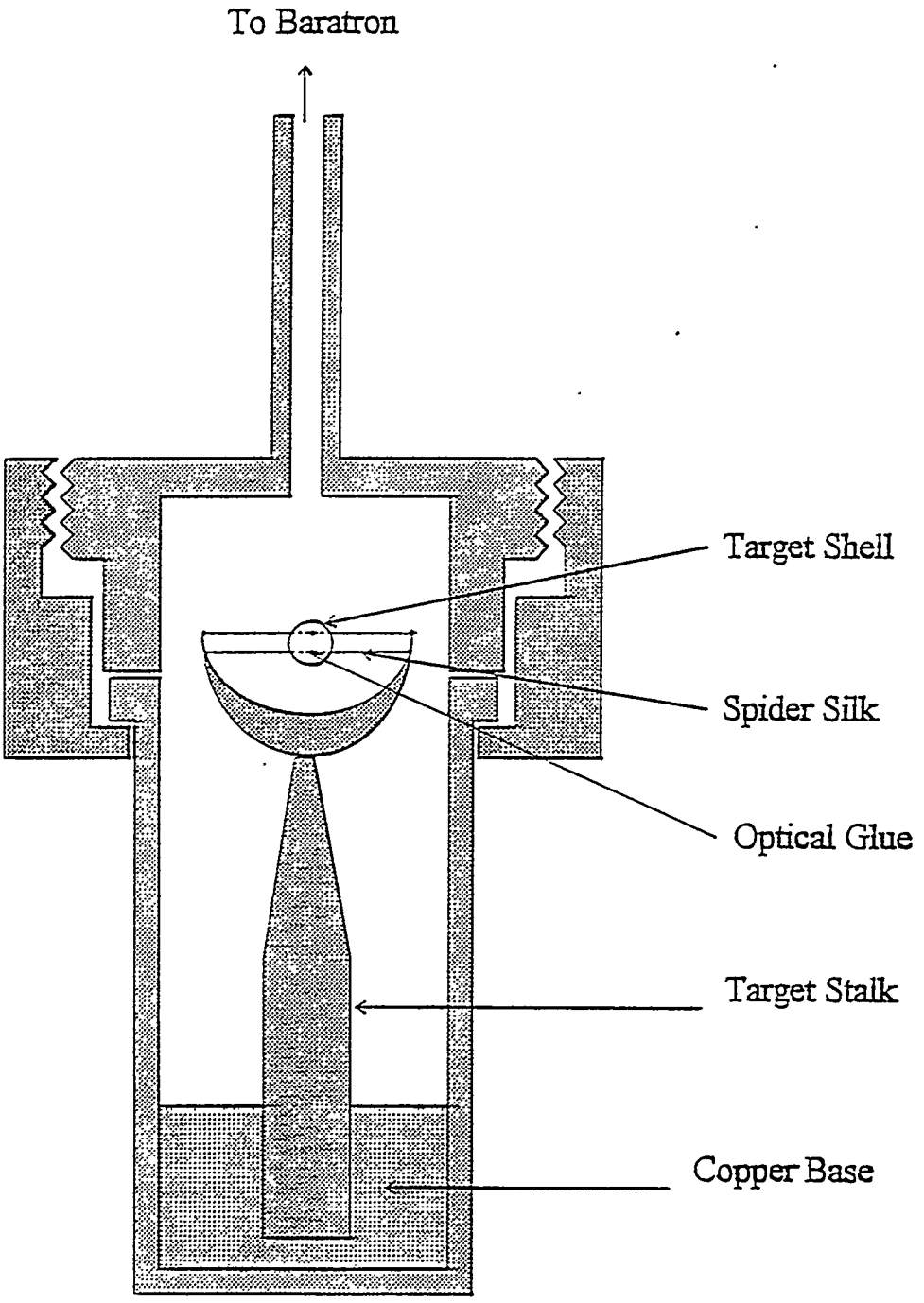

Fig.. 2. Sample cell with target shell glued to spider silks strung across a forked stork.

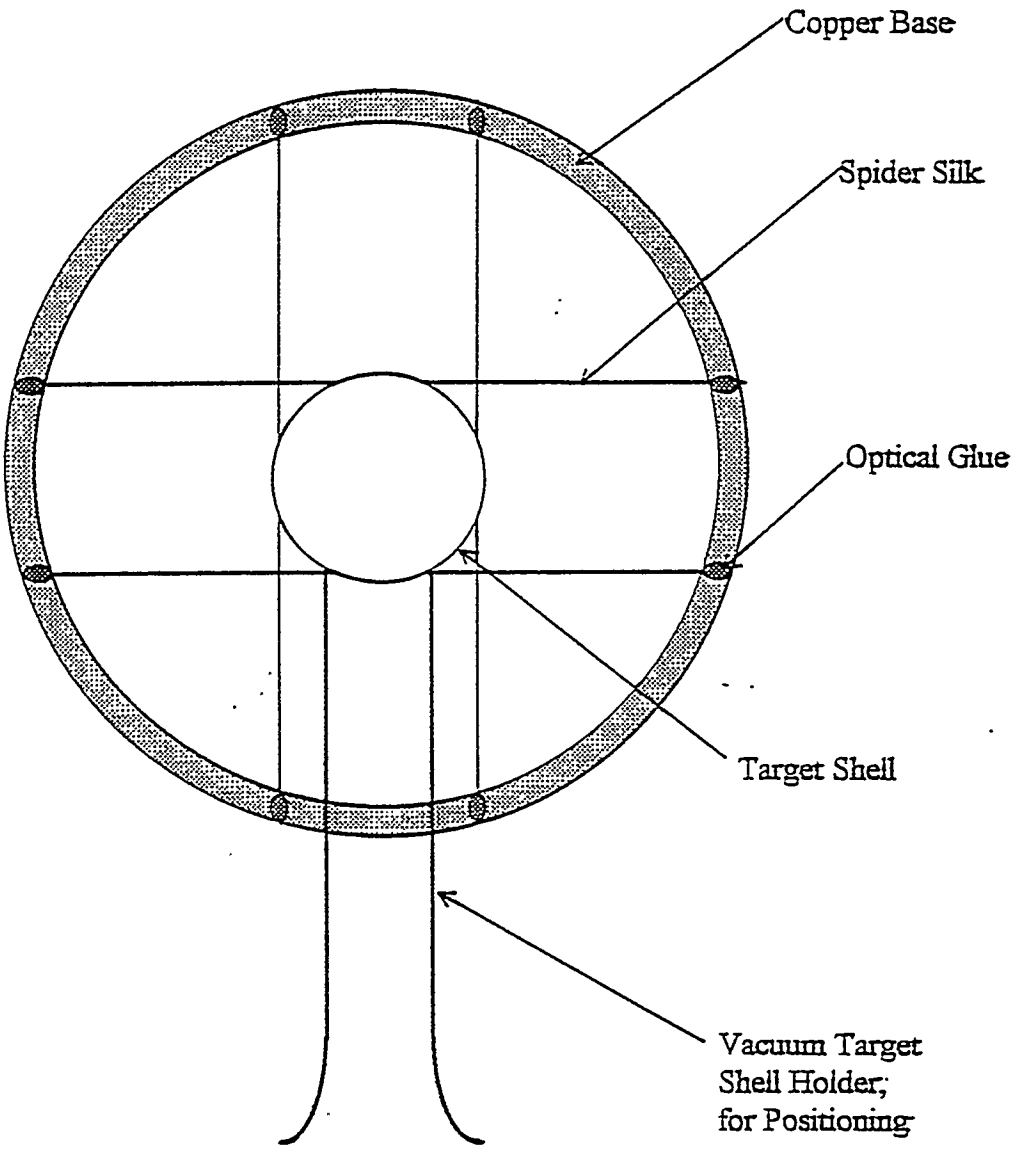

Fig. 3. Freely-resting target shell on a spider-silk net.

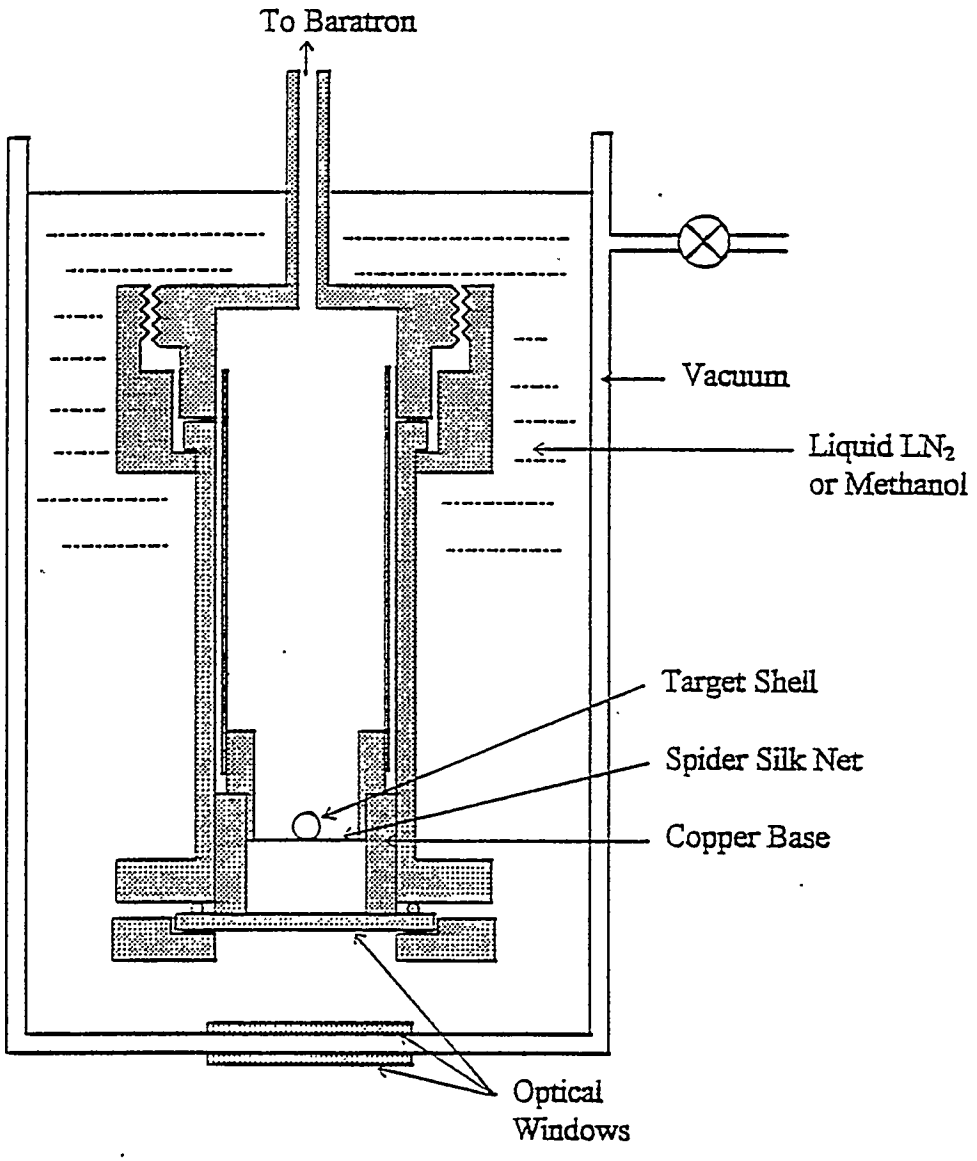

Fig. 4. Sample cell and temperature stabilization bath with optical access. Target shell is freely positioned on the spider silk net. Temperature range is 77 - 350K.

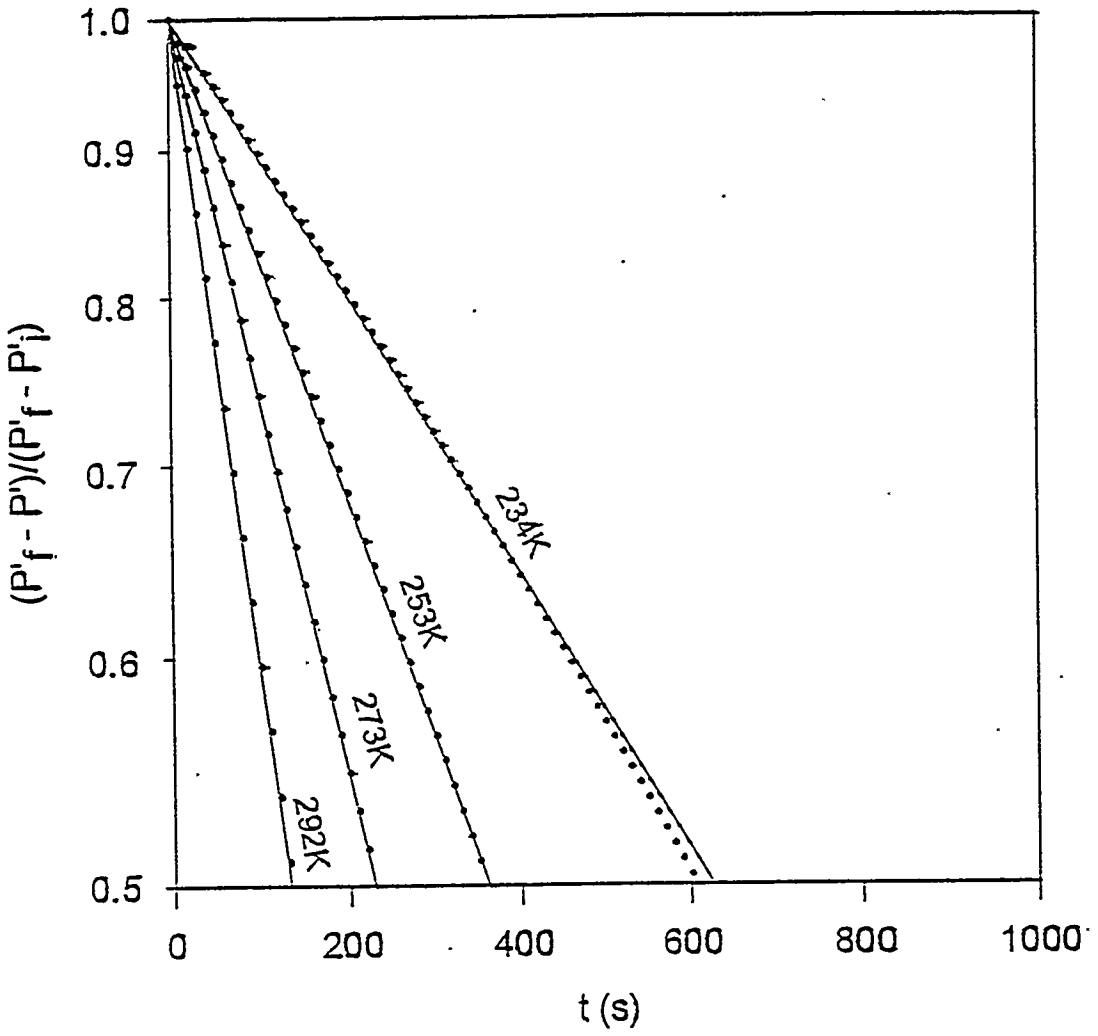

Fig. 5. Semi-log plot of leakage of high pressure helium gas out of shell 1S into sample cell, which is at very low pressure. Solid lines represent least square straight line fit to the data, in accord with Eq. (3). P′ is baratron pressure corrected for background (desorbed) gas from sample cell walls. P'_i and P'_f are initial and final corrected pressures. Shell 1S has a smooth surface as viewed with an optical microscope. Its parameters are: OD = 945 μm, wall thickness = 17 μm, weight = 50.1μg.

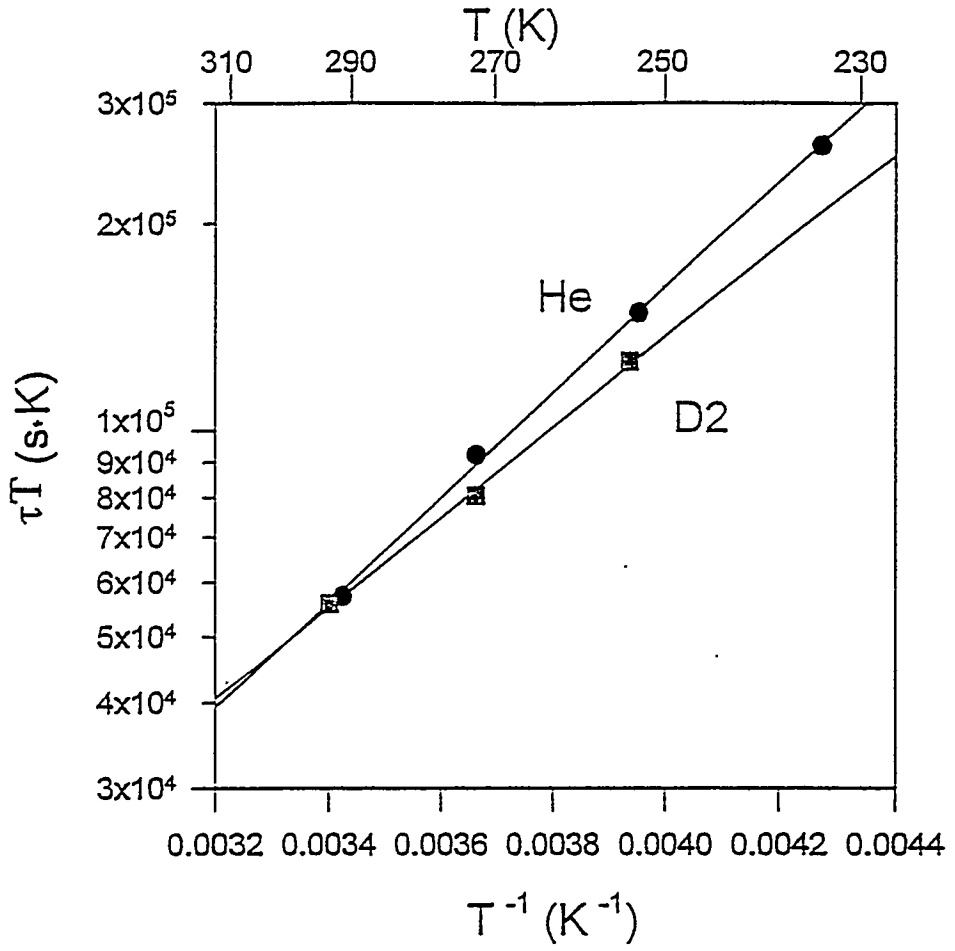

Fig. 6. Activation type dependence of permeation time constant on T^{-1}, as indicated in Eq. (4). Shell 1S parameters are: OD = 945 μm, wall thickness = 17 μm, weight = 50.1μg. Slope gives the permeation constant, K_P. The plot serves as a means of obtaining the shell temperature, T_S, from the permeation time constant τ.

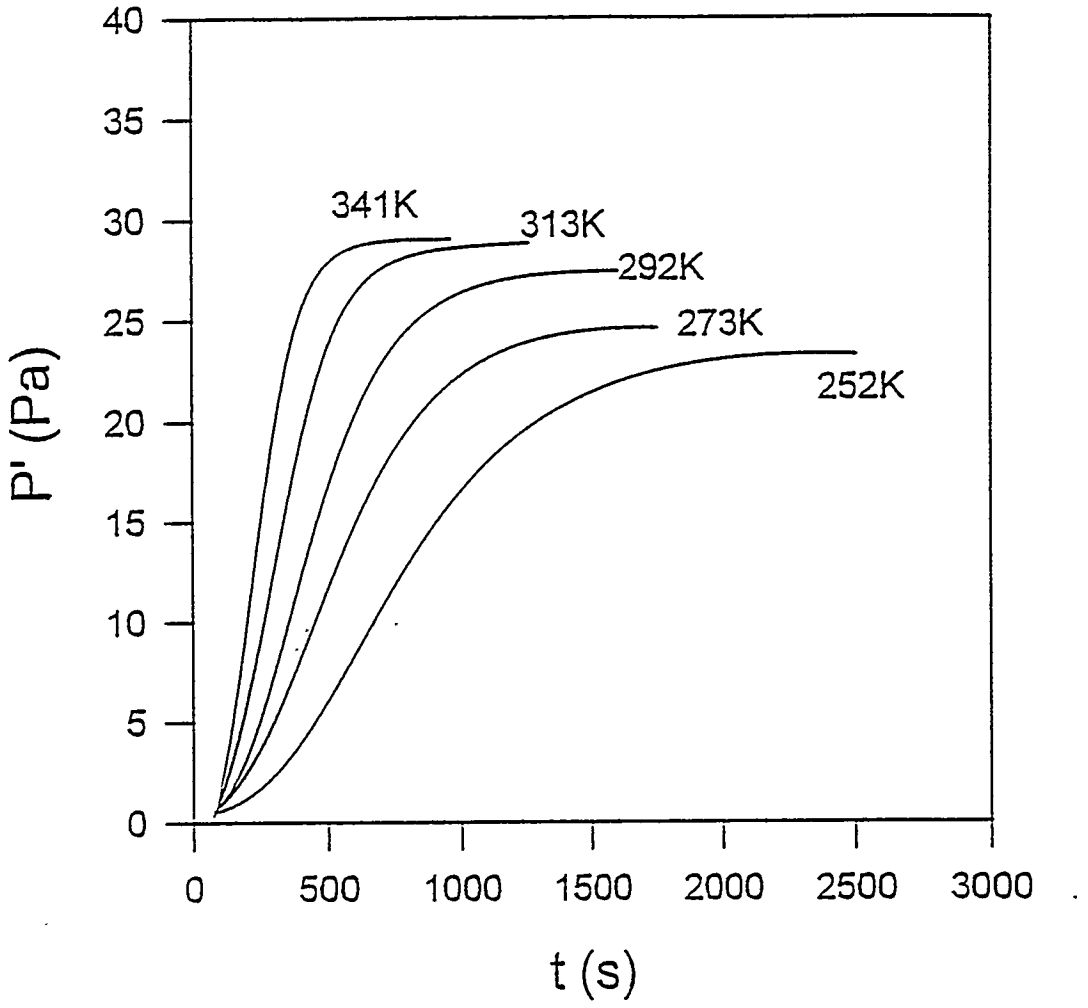

Fig. 7. Increase of pressure, corrected for background, in sample cell, due to helium gas permeation out of shell 1S during warm-up. Shell 1S parameters are: OD = 945 μm, wall thickness = 17 μm, weight = 50.1μg. Initial shell pressure is 12 atm.

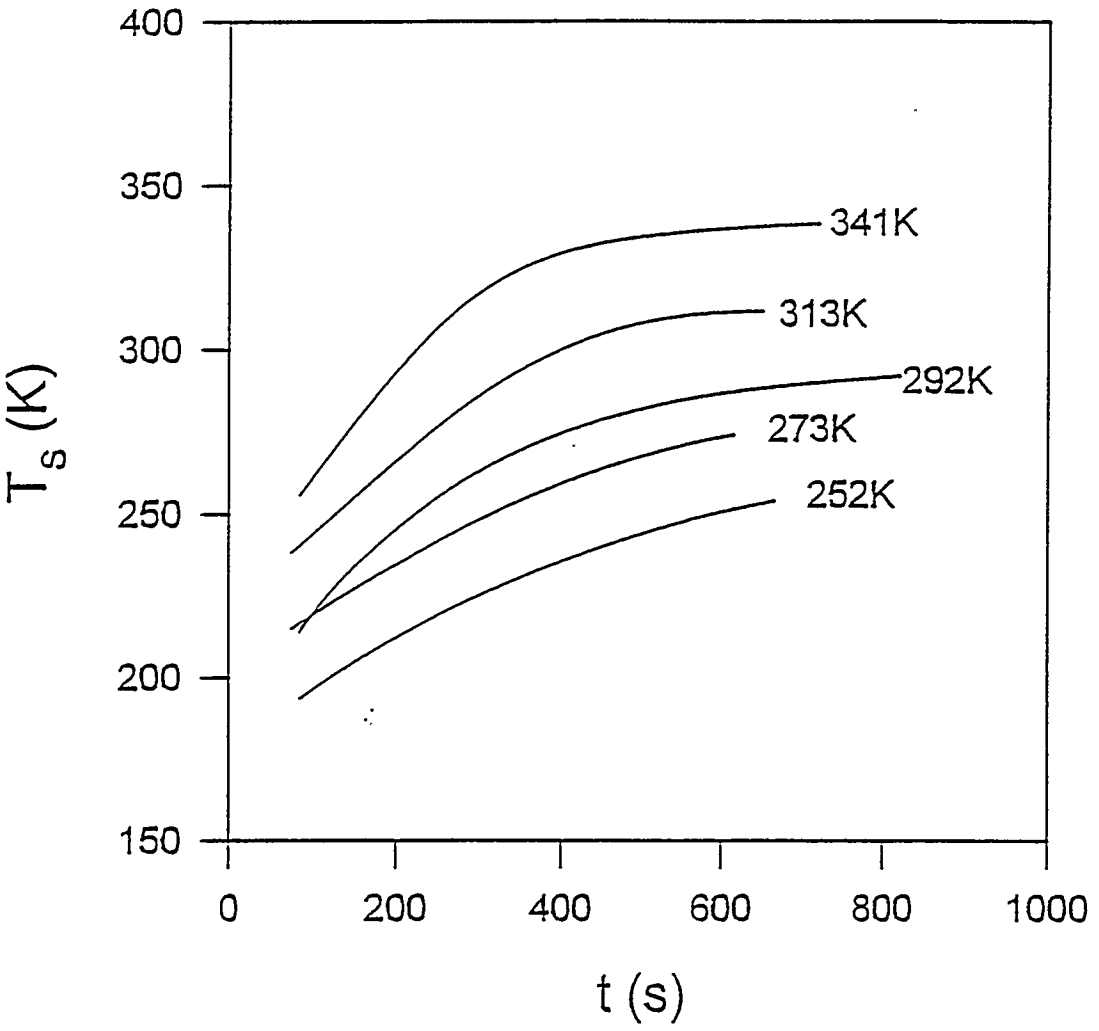

Fig. 8. Temperature rise of shell 1S during warm-up procedure. T_S at time t is calculated from dP′/dt data, which is plotted in the previous figure (Fig. 7). See text for details.

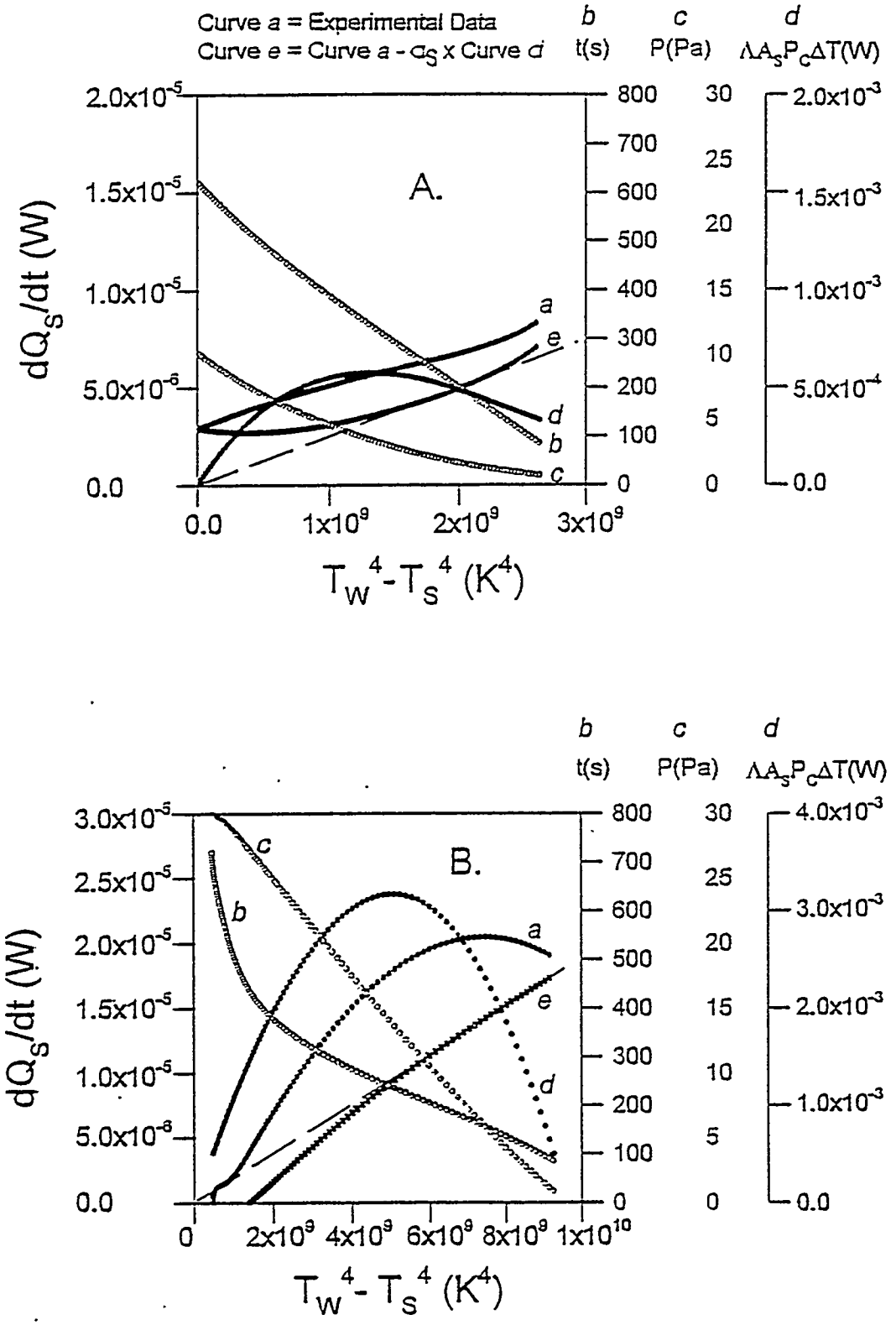

Fig. 9. Emissivity and accommodation coefficient determinations using a graphical method for shell 1S, filled with helium gas, and at two wall temperatures, the lowest and highest ones used in in the preceding three figures. Shell 1S parameters are: OD = 945 μm, wall thickness = 17 μm, weight = 50.1μg. **A.** T_W = 252 K. e_S = 0.016, a_S = 0.0037. **B.** T_W = 341 K. e_S = 0.012, a_S = 0.0027. See text for explanation of how e_S and a_S are determined.

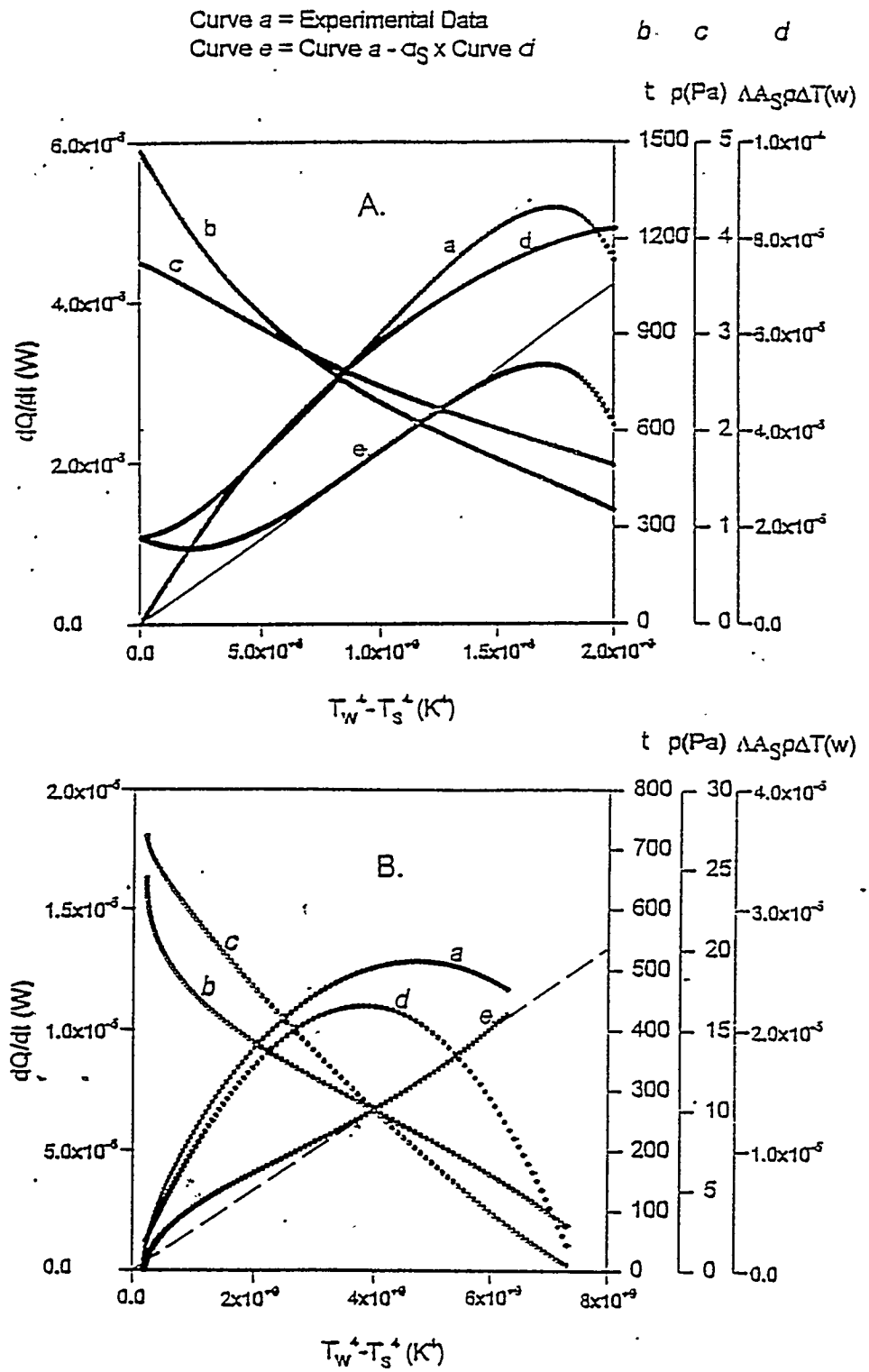

Fig. 10. Emissivity and accommodation coefficient determinations using a graphical method. **A.** Brominated polystyrene shell Br-30. $T_W = 315K$, helium gas is shell. Shell parameters are: OD = 660 μm, wall thickness = 147 μm, weight = 134.9 μg. $e_S = 0.025$, $a_S = 0.025$. **B.** Shell 1S for comparison, at a comparable $T_W = 313K$, helium gas in shell. See caption of Fig. 9 for shell parameters. $e_S = 0.011$, $a_S = 0.0028$. The emissivity in A is about double that of B, understandable in terms of the wall thicknesses, and a_S of 'rough-surface' shell Br-30 is almost an order of magnitude larger than that of smooth shell 1S.

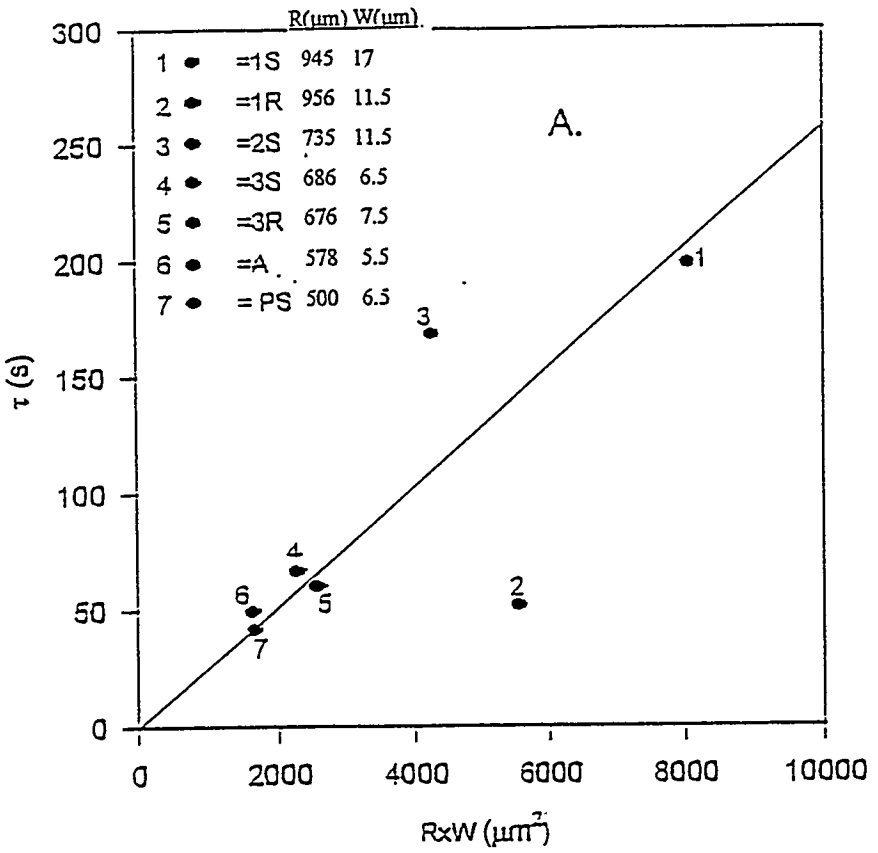

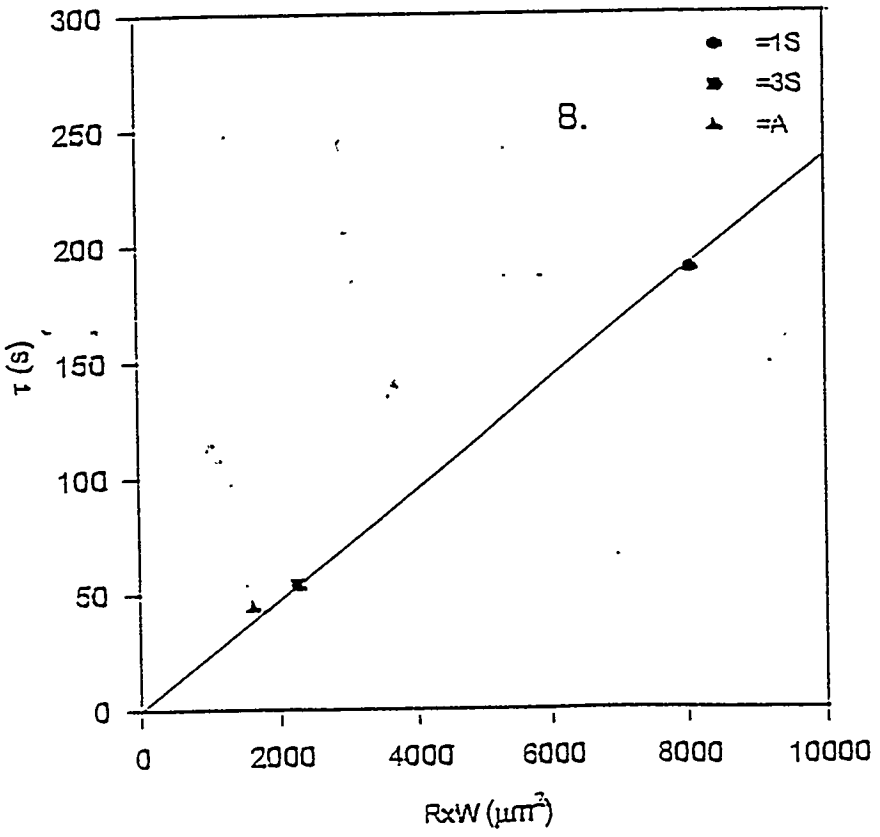

Fig. 11. Permeation time constant at 293K as a function of (Radius X Wall Thickness) for polystyrene shell. According to Eq. (6), the experimental points should lie on a straight line whose slope is proportional to K_P (293K). A. Helium gas. B. D_2 gas. Shells 1R and 2S have anomalous "effective" K_P's. See text for comments.

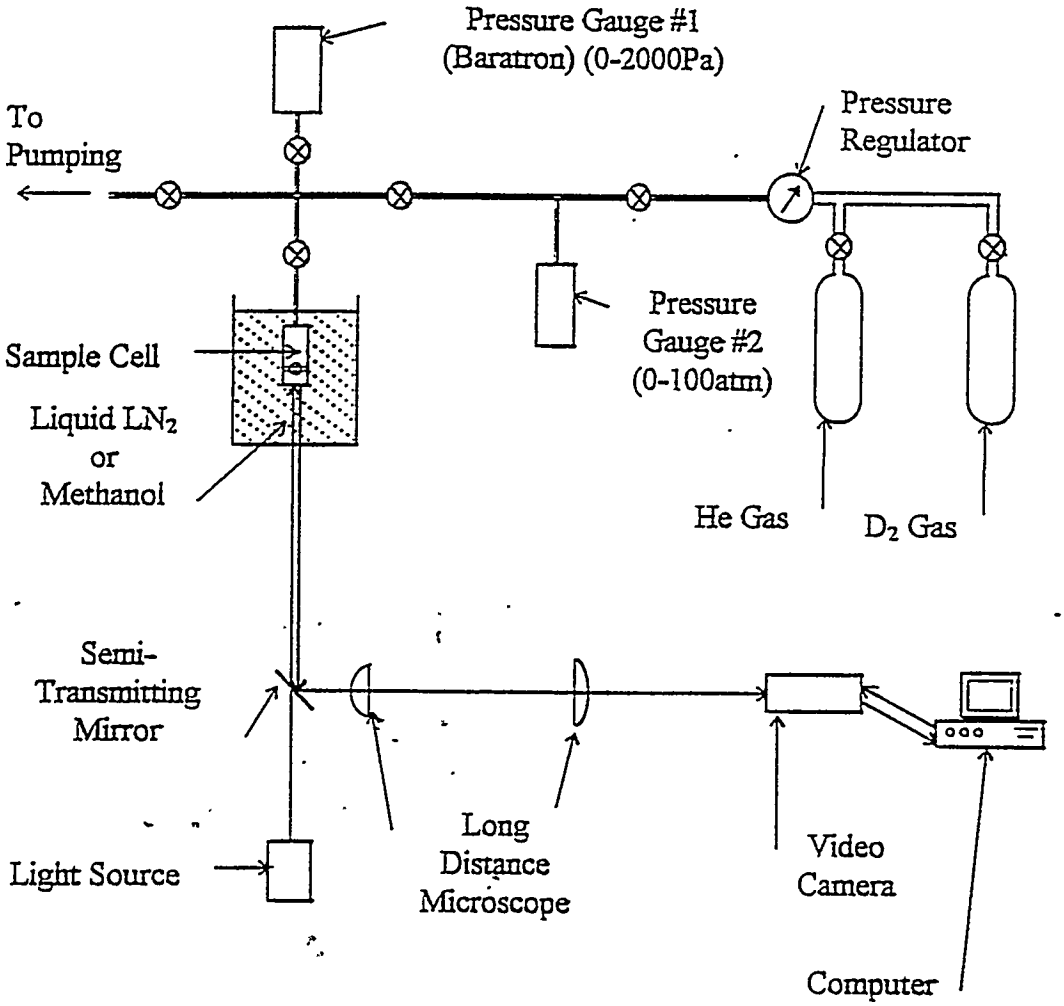

Fig. 12. Visually accessible permeation experimental apparatus shown with long distance microscope. See Fig. 4 for details of sample cell and surrounding temperature bath.

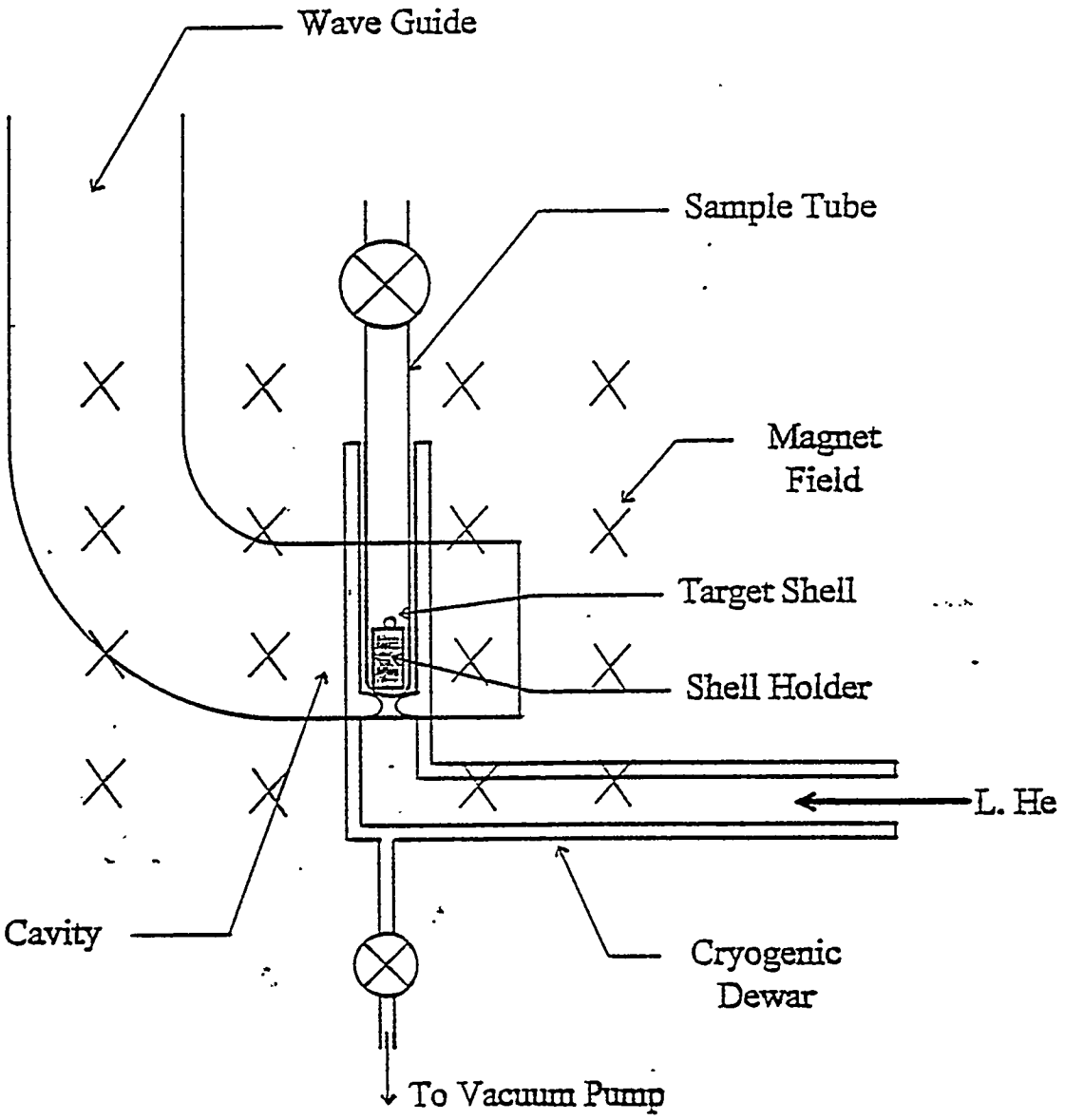

Fig. 13. Microwave cavity section of X-band ESR Spectrometer with continuous flow liquid helium cooling.

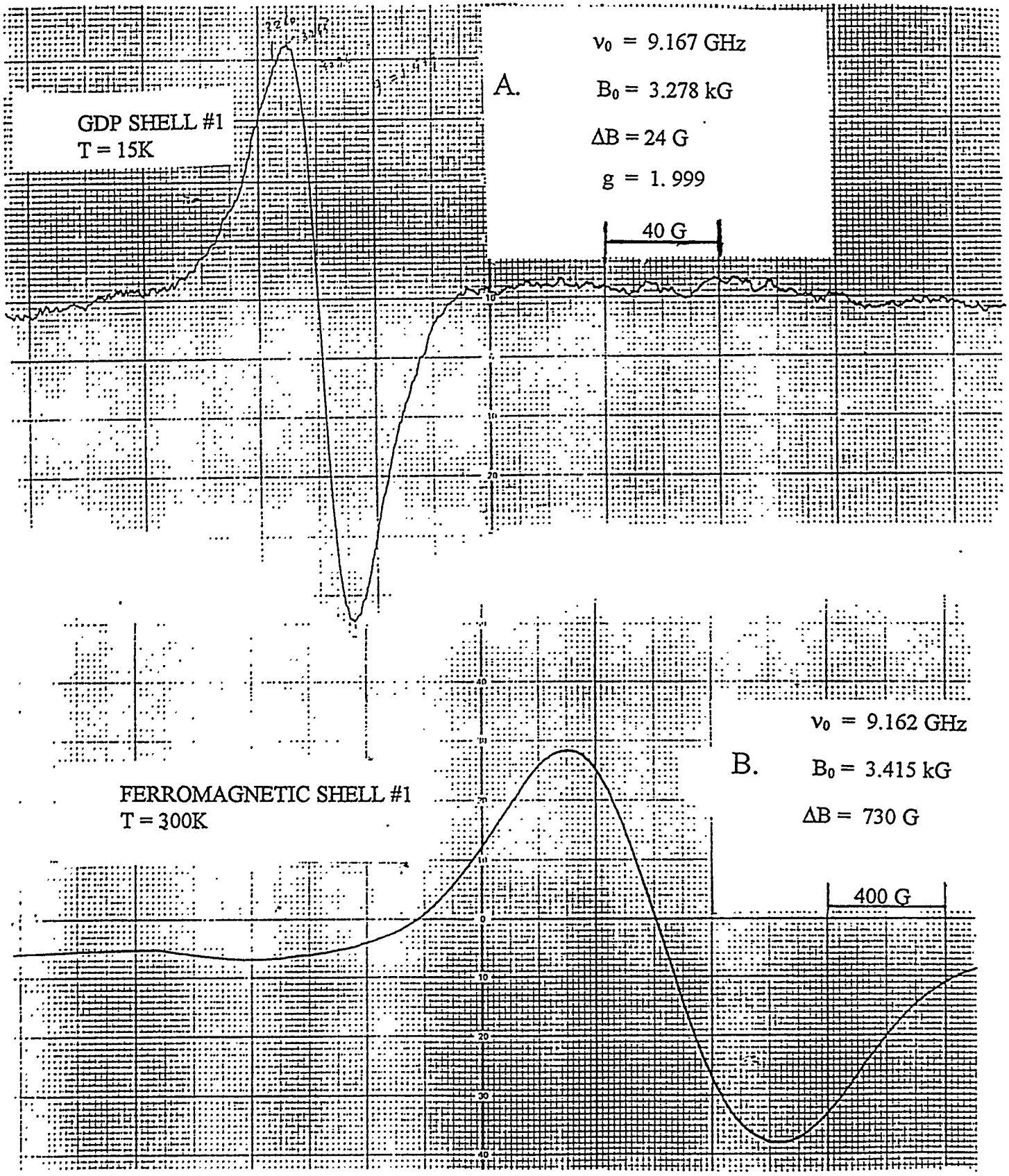

Fig. 14. ESR signals for magnetic shells. A. Fresh GDP plasma coated shell. Equilibrium magnetization obeys Curie law throughout 7K - 200 K temperature range used. B. Shell formed in drop tower, using styrene doped with 10 nm diameter magnetite particles. The magnetization is saturated and the ESR signal is approximately temperature independent in the investigated range 15K - 300K.